ASIAN JOURNAL
OF ORGANIC CHEMISTRY

www.asianjoc.org

Accepted Article

Title: π-π Interactions: Influence on molecular packing and solid state emission of ESIPT and non-ESIPT motifs

Authors: Shu Seki; Vikas Padalkar; Daisuke Sakamaki; Kenji Kuwada; Akifumi Horio; Haruka Okamoto; Norimitsu Tohnai; Tomoyuki Akutagawa; Ken-Ichi Sakai

To be cited as: Asian J. Org. Chem. 10.1002/ajoc.201600159

Link to VoR: http://dx.doi.org/10.1002/ajoc.201600159

A Journal of

ACES
Asian Chemical Editorial Society

A sister journal of **Chemistry – An Asian Journal** and **European Journal of Organic Chemistry**

WILEY-VCH

FULL PAPER WILEY-VCH

π–π Interactions: Influence on molecular packing and solid state emission of ESIPT and non–ESIPT motifs

Vikas S. Padalkar,*[a] Daisuke Sakamaki, [a] Kenji Kuwada, [a] Akifumi Horia, [a] Haruka Okamoto, [a] Norimitsu Tohanai, [b] Tomoyuki Akutagawa, [c] Ken-ichi Sakai, [d] and Shu Seki*[a]

Abstract: Novel, triphenylamine (TPA)– benzothiazole (BZT) based excited state intramolecular proton transfer (ESIPT) and non–ESIPT fluorescent motifs have been prepared by Suzuki coupling reaction. The photophysical properties in solution, aqueous suspension, and in solid state were systematically investigated. High fluorescence quantum efficiencies (Φ_{sol}: ~ 95%; Φ_{solid}: ~ 88%), moderate stokes shift (~8,000 cm^{-1}), microenvironment sensitive, and molecular framework dependent emission are the striking features of the present protocol. Solid state emission was modulated and interpreted via cross–over effect of π–π interactions using single crystal X–ray analyses. Non–planar/ twisted framework in the system helps to avoid non–covalent interactions, facilitating the suppression of fluorescence quenching in the solid state with high quantum efficiency over 88 %.

Introduction

Photoluminescent organic solid–state materials have been attracting considerable interest in optical devices[1],[2] such as organic light emitting diodes[3], data recording/ storage devices[4], and security printing[5]. Easy synthesis, photostability, color purity, and high luminescence quantum efficiency are the essential factors for the development of new luminescent compounds. Solid state emissive properties of the organic chromophores depend on structure of the chromophores, crystal packing, intermolecular and intramolecular interactions[6–13]. Different intermolecular interactions such as π–π stacking, hydrogen bonding (C–H…O, C–H…π, C–H…N, O–H…N), and non–covalent forces determine the fluorescence quantum efficiency of the chromophores in the solid state[14–17]. Strong intramolecular interactions in the ESIPT chromophores enhance the fluorescence quantum efficiency[2,18], while intermolecular interactions quench the fluorescence in the solid state[16]. The fluorescence properties of compounds in the solid state are tunable by controlling the π–π stacking and hydrogen bonding via altering substitution pattern[2,18,19]. Understanding the role of interactions that determine the packing of molecules in the solid state and how they affect the optical properties of the materials is therefore essential for tuning their solid state emission properties.

In recent years, donor–π–acceptor (D–π–A) structured luminogens have been the thrust area of research because of their optical and electronic properties can be facilely modulated through tuning the (i) electron donor and/or acceptor strength (ii) length of π–system (iii) conformational changes[20]. D–π–A chromophores exhibiting broad and intense absorption spectra[21], are proposed as one of the most promising candidates in organic photovoltaics[22]. Stimuli–responsive emission switching of D–π–A chromophores in solid state/ aggregate state have been attracting increasing attention owing to their fundamental importance and potential applications in sensing devices[23,24].

In present study triphenylamine (TPA) has been chosen as an electron donor unit and benzothiazole (BZT) as electron acceptor unit. TPA is a non–planar unit, because of its non–planar characteristic it can prevent interaction or close stacking[20,23]. BZT unit helps to achieve the solid state emission by reducing the self absorption[25,26]. Based on this idea, we have synthesized D–π–A type of chromophores **I**–**III** (**Fig 1**), and examined the relationship between solid–state fluorescence quantum efficiency and molecular packing systematically.

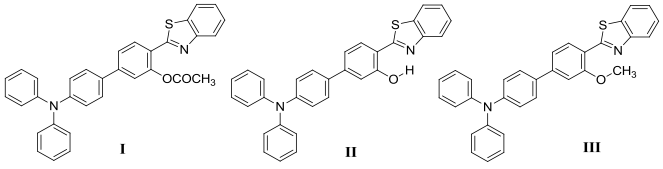

Figure1. Structure of compounds **I–III**

Results and Discussions

Compounds **I–III** were synthesized by the Pd–catalyzed Suzuki coupling reaction between 2–(benzo[*d*]thiazol–2–yl)–5–bromophenyl acetate and 4–(diphenylamino)phenyl boronic acid in good yields **Scheme1**. Intermediate **4** was prepared from 2–aminothiophenol **1** and 2–hydroxy–4–bromobenzoic acid **2** by acid catalyzed cyclization followed by acetylation reactions. Intermediate **4** was coupled with 4–(diphenylamino) phenyl boronic acid **5** via Suzuki coupling reaction using $Pd(PPh_3)_4$ under alkaline condition to obtain compound **I**. The compound **I** was treated with

[a] Dr. V.S. Padalkar*, Dr. D. Sakamaki, Mr. K. Kuwada, Mr. A. Horio, Ms. H. Okamoto and Prof.(Dr). S. Seki*
Department of Molecular Engineering
Kyoto University
Katsura Campus, Kyoto-615-8510, Japan.
E-mail: vikaspadalkar@gmail.com (V.S.P);
seki@moleng.kyoto-u.ac.jp (S.S)
[b] Dr. N. Tohanai
Department of Material and Life Science
Osaka University
Suita Campus, Suita, Osaka 565-0871, Japan
[c] Prof. (Dr.) T. Akutagawa
Institute of Multidisciplinary Research for Advanced Materials
Tohuku University
Sendai, 980-8577, Japan
[d] Dr. K. Sakai
Department of Bio-& Material Photonics
Chitose Institute of Science and Technology
Chitose 066-8655, Japan

Supporting information for this article is given via a link at the end of the document.

potassium hydroxide in dichloromethane at reflux temperature to obtain **II** with good yield. Compound **II** on methylation by using NaH yields compound **III**. The intermediate **4**, and compounds **I**–**III** were purified by column chromatography followed by HPLC and well characterized by elemental analysis, NMR spectroscopy and mass spectrometry.

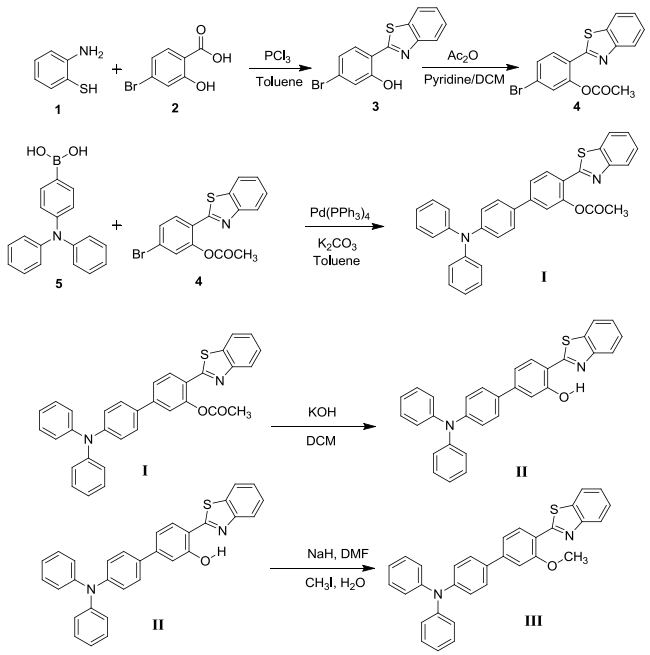

Scheme 1. Synthetic route for the compounds **I** and **II**

The absorption, excitation, emission, and fluorescence quantum efficiencies of the compounds **I**–**III** in the solid state and in solvents of different polarities are summarized in **Table 1**. Compounds exhibit strong absorption band between 290 and 380 nm in different solvents, which can be assigned to the π–π* transition of the TPA–BZT backbone. In studied solvents, the spectral position of the absorption bands was almost same, which indicates the little influence of solvent polarity on the ground state of the molecules (**Fig 2** and **Fig S1**). The insensitivity of the absorption spectra of these molecules to the solvent polarity indicates that dipole moment of compounds in the ground state is nearly identical[6]. The compound **I** showed red shifted absorption (λ_{abs} = 380 nm) in dimethyl sulfoxide (DMSO) in comparison to other studied solvents. However, compound **II** showed red shifted absorption in chloroform (λ_{abs} = 385 nm).The absorption spectra of compound **III** is almost identical to absorption spectra of compound **I**.

Interestingly, the emission properties of the compounds are solvent dependent (**Fig 2** and **Fig S2**)**.** In polar solvents (acetonitrile, methanol, and DMSO), compounds showed red emission in comparison to emission in non–polar solvents (toluene, tetrahydrofuran (THF), and chloroform) indicating change in the dipole moment at the excited state. Compounds show large positive solvatochromism in fluorescence, from 443 nm in toluene, to 530 nm in methanol for compound **I**, 444 nm in toluene, to 527 nm in acetonitrile for compound **II**, and from 432 nm in toluene to 508 nm in methanol for compound **III (Fig S2)**. These result clearly indicate that the dipole moment of the emissive species are significantly higher compared to that of their ground state[6]. The excitation spectra of the compounds were recorded and results show that spectra are almost identical for all studied compounds (**Fig S3**). Compounds **I**–**III** show broad emission in different solvents and red shift with solvent polarity (**Fig 2**). This red shift can be assigned to intramolecular charge transfer emission. As compound **II** contains ESIPT unit, it was expected to have different emission pattern (single broad emission or dual emission i.e. ESIPT emission) compared to compounds **I** and **III** (Intramolecular charge transfer emission) in solution and solid state.

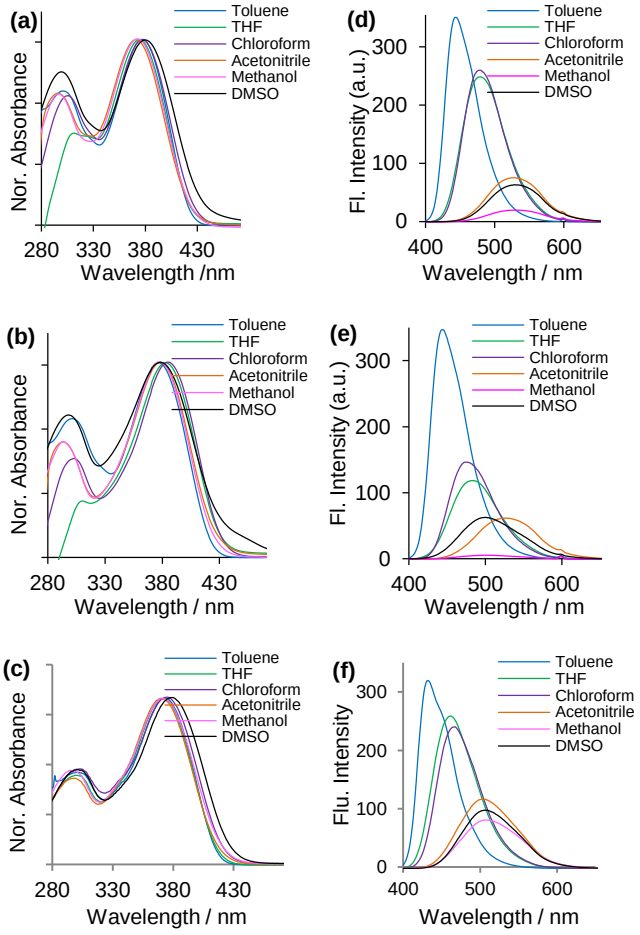

Figure 2. Steady state absorption (a,b,c) and emission (d, e, f) spectra of compounds **I**, **II** and **III** respectively in different solvents (10^{-5} M concentration) at room temperature, λ_{ex}: 370 nm.

Table 1. Summary of optical properties of the compounds **I**–**III**

Comps	Medium	λ_{max}^{Abs} (nm)	ε (mol^{-1} dm^3 cm^{-1})	λ_{max}^{Ex} (nm)	λ_{max}^{Em} (nm)	Stoke shift (nm)	Stoke shift (cm^{-1})	Quantum efficiency Φ_f (%)
I	[a] Solid Film	408	*e*	398	480	72	3676	[c] 74
	[b] Toluene	378, 301	60800 43900	372 309	443	65	3881	[d] 88
	[b] THF	375, 313	66700 33000	372 308	478	103	5746	[d] 90
	[b] Chloroform	377, 305	57000 39800	373 307	470	93	5248	[d] 88
	[b] Acetonitrile	370, 296	42400 30200	369 304	525	155	7979	[d] 78
	[b] Methanol	371, 296	19200 13600	370 303	530	159	8086	[d] 40
	[b] DMSO	380, 299	49600 41000	373 308	528	148	7376	[d] 78
II	[a] Solid Film	350	*e*	370	465 527	115	7066	[c] 22
	[b] Toluene	376, 302	60700 43200	374 306	444	68	4073	[d] 37
	[b] THF	382, 310	53600 15500	373 303	483	101	5474	[d] 65
	[b] Chloroform	385, 303	49100 24800	373 306	475	90	4921	[d] 66
	[b] Acetonitrile	379, 293	50300 29800	371 301	527	148	7409	[d] 70
	[b] Methanol	378, 294	15900 9400	366 303	500	122	6455	[d] 15
	[b] DMSO	380, 298	37100 27100	369 307	500	120	6315	[d] 80
III	[a] Solid Film	388	*e*	400	467	79	4359	[c] 88
	[b] Toluene	372 300	66400 36900	369 308	432	60	3733	[d] 81
	[b] THF	371 299	70500 37800	368 305	461	90	5262	[d] 87
	[b] Chloroform	375 303	65600 37400	370 308	466	91	5207	[d] 85
	[b] Acetonitrile	370 299	70500 36600	368 304	503	133	7146	[d] 80
	[b] Methanol	371 297	68000 38500	369 304	508	137	7269	[d] 64
	[b] DMSO	380 302	65500 37100	371 307	506	126	6552	[d] 95

[a] Measured on thin film, spin-cast from (1 wt %) dichloromethane solution. [b] Measured from 10^{-5} M solution. [c] Absolute quantum yields in solid state. [d] Quantum yields in solution (10^{-5} M). [e] Not calculated.

However, the emission pattern of the compounds **I, II** and **III** are almost identical in studied solvents (non-polar, moderately polar and polar solvents). In non–polar solvents (toluene and chloroform), emission maxima is between 430 and 480 nm, red-shifted gradually in moderately polar solvent (THF; between 461– 483 nm) and in polar solvents (acetonitrile, methanol and DMSO; between 500–530 nm). The identical emission pattern of the ESIPT compound **II** and non–ESIPT compounds **I** and **III** in solution concludes that the emission of the compound **II** in solution would be due to ICT rather than ESIPT mechanism. Recently, similar observations have been reported by our group for triphenylamine-benzothiazole (donor-acceptor) based ESIPT and non-ESIPT chromophores. Similar to solution, compounds are highly emissive in the solid state (**Fig 3**). However, the emission pattern for ESIPT (compound **II**) and non-ESIPT compounds (compounds **I** and **III**) are completely different. Compounds **I** and **III** exhibit yellow ICT (intramolecular charge transfer) emission λ_{em} = 480 nm, 467 nm with 74% and 88% fluorescence quantum efficiency respectively, while compound **II** showed dual emissions (λ_{em} = 465, 527 nm) with 22% quantum efficiency (**Fig 3**).The dual emission for the compound **II** is assigned to excited state intramolecular proton transfer (ESIPT) process. The short wavelength (λ_{em} = 465) and long wavelength emission (λ_{em} = 527nm) can be assigned to the excited state *cis*–enol and *cis*–keto tautomer respectively[27]. The dual emission in the solid state for ESIPT compound could be due to restriction of *cis*–*trans* transformation of the keto form in the

excited state due to tight molecular packing[28–31]. In the solid state intramolecular hydrogen bond facilitates over intermolecular hydrogen bonding due to physical constraint resulted into ESIPT process[18]. ESIPT emission in condensed phase was further supported in aggregation induced emission (AIE) study.

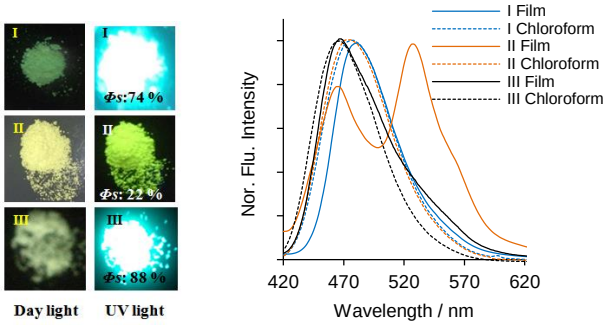

Figure 3. (left) Day light and UV light images of compounds **I–III**; (right) Emission spectra in solid state (spin coated: 1wt %) and in chloroform (10^{-5}M conc. at room temp., λ_{ex}: 370 nm).

The striking features of these compounds are moderate Stokes shift (~8,000 cm^{-1}) and very high fluorescence quantum efficiency in solution (Φ_f ~95%) and solid state (Φ_f ~88%) (**Table1**). The significant intramolecular charge transfer (ICT) in the excited state could be the probable factor for moderate Stokes shift for the compounds [32] in solutions and ESIPT process[2,18,26] for compound **II** in solid state. High fluorescence quantum efficiency in solution is a common characteristic of the donor–acceptor type of chromophores[33–36]. Red shifts of emission spectra with fluorescence quenching in the solid state are the most common limitations of the reported donor-acceptor system[37] which were overcome by present compounds **I** and **III**. The fluorescence quantum efficiencies and emission spectra of the compounds **I** and **III** in the solid state and solution are comparable. However, significant difference was observed for compound **II** in the solid state and some solvents. The quenching of the fluorescence quantum efficiency of the compound **II** can be assigned to molecular conformation, which was further discussed in detail by single crystal study. In bulk material, optical properties can be tuned by controlling intermolecular interactions which lead to formation of aggregates or planarization effect[38]. In present case, to understand the relation between molecular packing and fluorescence quantum efficiencies in the solid state, aggregation induced emission (AIE) and single X–ray crystal analyses study were performed for compounds **I** and **II**.

The AIE study was performed in THF: water mixture (various ratios) with the help of absorption and fluorescence spectroscopy (**Fig 4**, **Fig S4** and **Fig S5**). In pure THF solution, compounds **I** and **II** show emission at 480 nm and 484 nm respectively. Upon increasing water fraction up to 70%, a significant gradual red shift of 46 nm (λ_{em} = 526 nm) for **I** and 43 nm (λ_{em} = 527 nm) for **II** with a decrease in fluorescence intensity was observed (**Fig 4**, **Fig S5** and **Table S1**). This change in the emission is not due to AIE but due to increased polarity of the solvents and stabilization of charge transfer state[19,39,40]. When water fractions were further increased from 70 to 95 %, significant blue shift in emission maxima was observed for the compounds with slight increase in fluorescence intensity (**Fig 4**). The blue shift in emission spectra is assigned to formation of nanoaggregates by suppression of intramolecular charge transfer process[41]. Emission maxima are blue shifted at higher fraction of water due to the elimination of solvent polarity effect in the aggregated state[41]. The sudden change in the absorption and emission spectra suggests the formation of nanoaggregates, i.e. transition from homogenous solution to the nano–particles[19,39]. In aggregate state, fluorescence intensity is high at 80% and 90% water fraction, but it again slightly decreases at 90 and 95 % water fraction for compounds **I** and **II** respectively. This can be assigned for phase change, i.e. more ordered nanoscale aggregates (crystalline) to random agglomerate at high percentage of water[37]. This observation supports the well know mechanism for emission properties[42], i.e. crystalline particles enhances the fluorescence while amorphous particles lead to quenching of fluorescence[42]. This observation was supported by atomic force microscopy (AFM) analysis for compound **I** (**Fig S6**). At lower fraction of water (10–60%) the emission spectra for both the compounds were almost identical (ICT emission), while at higher fraction of water (70–95%) emission properties of the compounds were significantly different, which indicates the occurrence of different emissive pathways at the excited state. The emission properties of the compounds **I** and **II** in the solution, solid state and aggregated state concludes that emissions of the compound **I** and **II** in aggregated state could be due to ICT or ESIPT process. The emission spectra of the compound **I** at higher fraction of water were identical to emission spectra of the compound **I** in solution which indicates that in aggregated state emission is ICT emission. However, in case of compound **II**, emission spectra in the solid state and aggregated state were identical, which indicates ESIPT emission.

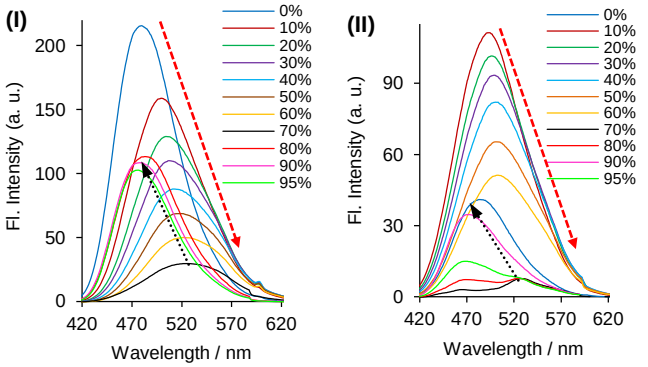

Figure 4. Emission spectra of compound **I** (left) and **II** (right) in THF and THF–water mixture (10^{-5} M concentration, room temperature, λ_{ex}: 370 nm, water fraction (vol%))

When the water fraction (f_w) is 70–95%, compound **II** shows significant ESIPT emission (**Fig S5**). In aggregate state, enhancement of emission can be assigned to RIR/ ESIPT process[2,18]. Thus, AIE study provides enough evidence for AIE active property of compounds. Compounds **I** and **II** contain same electron donor and acceptor groups only the substituents at 2–position on BZT unit are different. This small structural change causes significant difference in fluorescence efficiency in the solid state. To gain insight into the fluorescence properties, single crystal study was performed for both the compounds.

Single crystals of the compounds were developed in mixture of chloroform and ethanol at room temperature. Their crystal data are summarized in SI (**Table S2** and **S3**). Compound **II** has eight molecules per unit cell which are slipped anti–parallel (**Fig 5**, right). Four molecules are independent exhibited in two pairs in the form of dimer with their dipoles pointing in opposite directions (**Fig 5**, left). The two dimers are exactly anti–parallel with head–to–tail pattern while two monomers are parallel with slight twisting (**Fig 5**). The distance between two dimers is ~3.4 Å, and the distance between the monomers in each dimer is between 3.8 to 4.4 Å. The **Fig 5** depicts that molecule A is surrounded by seven molecules with different type of alignments (**Fig S7**). In unit cell, molecules alignments are anti–parallel to each other in head–to–tail fashion/ parallel with face–face fashion (**Fig S7**). All the possible alignments presented in **Table S4** show different non–covalent interaction (π–π, C–H…π, C–H…O, C–H…N). However, π–π interaction (~ 3.4 Å) is very strong interactions over other non–covalent interactions. Quenching of fluorescence quantum efficiency of compound **II** in solid state can be assigned to presence of strong π–π non–covalent interaction. In ESIPT system, quantum efficiencies in the solid state depend on strength of intramolecular hydrogen bond and it is directly proportional to fluorescence quantum efficiency[2]. In compound **II** along with intramolecular (O–H…N) bonding, intermolecular interactions are also present in the system as confirmed by single crystal data (**Fig S7**).

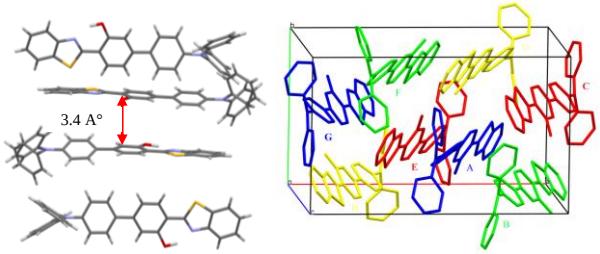

Figure. **5** (left) X–ray single crystal structure of compound **II** and (right) molecular packing arrangement of compound **II**. Thermal ellipsoids are set at 50% probability. Hydrogen atoms are omitted in molecular packing structure for clarity.

These non–covalent intermolecular interactions hamper the ESIPT process of compound **II** resulting in lowering of fluorescence quantum efficiencies in solid state[9,18]. In solution, these interactions are weak due to molecular motion, which results in high fluorescence quantum efficiencies due to ICT emission. The crystal structure of the compound **I** is shown in **Fig 6**. As shown in the **Fig 6**, compound **I** is not completely planar, the torsion between thiazole–phenyl and phenyl–phenyl are 8° and 24° respectively and TPA unit is completely outside the plane (θ = 42°) (**Fig S8**). This observation suggests that π–π interactions would be weaker in compound **I**. In molecular packing, four molecules are arranged in chair fashion, two molecules are in anti–parallel head–to–tail fashion which lie in one plane and two molecules are orthogonal to central molecules pointing out of plane. The intermolecular distance between two molecules is 4.2 Å which confirms the absence of or a very weak π–π stacking (**Fig S8**). These weak π–π and other non–covalent interactions can be assigned to steric acetyl group present in the framework. This observation supports the high quantum efficiency of the compound in solid state. Similar to compound **I** compound **III** also shows very high quantum efficiency (Φ_f = 88%) in the solid state. Co–planar conformation and weak non–covalent interactions could be the probable factors for high quantum efficiency. In order to conform molecular packing of compound **III** many attempts were performed to develop single but we are unable to obtain single crystal suitable for X–ray analysis. From above discussion we conclude that in bulk materials, a strong π–π intermolecular interaction quenches the fluorescence efficiencies, while weak π–π interaction enhances the fluorescence efficiencies [15].

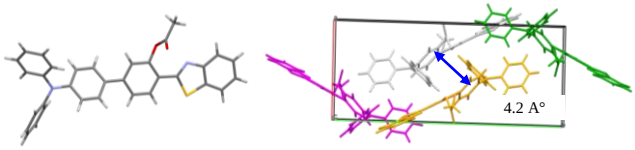

Figure 6. (left) X–ray single crystal structure of compound **I**, (right) molecular packing arrangement of compound **I**. Thermal ellipsoids are set at 50% probability.

Differential Scanning Calorimetry (DSC) analyses for the compounds were performed on neat material under nitrogen atmosphere to study the phase transitions (**Fig 7** and **Fig S9**). In first heating cycle very sharp melting endothermic transitions were observed at 193 ^{o}C and 229 ^{o}C for compounds **I** and **II** respectively, which indicates the presences of molecular order in the crystalline state. After melting transition compound **I** appear to be in glass state upto 300 ^{o}C and remains in glass state even after cooling to room temperature and also on further second heating and cooling cycle. However, compound **II** appears to be in glass state upto 300 ^{o}C and during the cooling process sharp exothermic phase transition was observed at 189 ^{o}C. This transition is phase change from amorphous state to crystalline state. Similar phase transitions were observed for compound **II** in second DSC heating and cooling cycle

(crystalline–amorphous–crystalline). This concludes that phase transitions of the compound **I** is irreversible in nature, but it is reversible for compound **II**. This can be assigned to more order molecular packing due to different strong non–covalent interactions present in compound **II**. The crystalline nature of the compounds was further confirmed by X-ray powder diffraction (powder–XRD) (**Fig 8**).

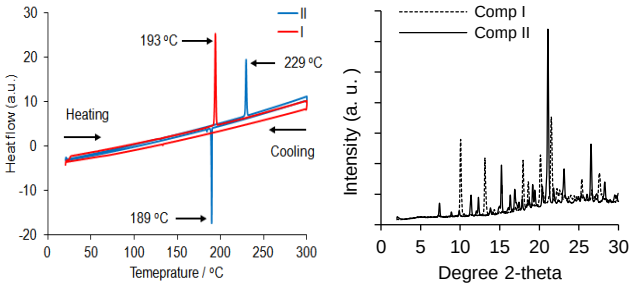

Figure 7. DSC data of compounds **I** and **II** (left)
Figure 8. Powder X-ray data of compounds **I** and **II** (right)

To have more understanding into the electronic structures of the compounds **I** and **II**, density functional theory (DFT) calculation was performed at the B3LYP/6–31G(d, p) level[43]. The molecular orbitals (only highest occupied molecular orbital (HOMO) and lowest unoccupied molecular orbital (LUMO) are presented here) of compounds are shown in **Fig 9**.

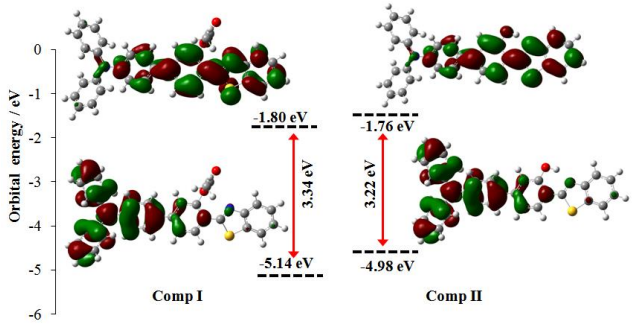

Figure 9. Frontier molecular orbitals with energies (HOMO and LUMO) of compound **I** and **II**

In both the cases HOMO orbitals are localized over TPA unit, whereas the LUMO orbitals are localized on the BZT unit. This clearly indicates that charger transfer from donor TPA unit to acceptor BZT unit occurs after photoexcitation. The difference between HOMO and LUMO for both the compounds are almost same, this also supports the evidence for identical absorption spectra of compounds.

Conclusions

In summary, we have investigated the relation between molecular packing and emission properties of the compounds in the solid state. Interestingly, slight change of substituent at 2–position of the BZT greatly affects the molecular packing and solid state behaviour. Strong π–π and other non–covalent interactions quench the fluorescence, while weak interactions enhance the fluorescence in the solid state. Steric acetyl group (**I**) and methoxy group (**III**) at 2–position of BZT hamper the ESIPT process resulted in single broad emission (ICT emission) in solution and solid state. Compound **II** shows ESIPT emission in solid and aggregated states due to physical constraint and absence of intermolecular hydrogen bonding with solvents. Enhancement of the fluorescence quantum efficiencies of compounds **I** and **III** in solid state is ascribed to weak non–covalent interaction due to co–planar conformations.

Experimental Section

Materials

Phosphorus trichloride, 4–bromo–2–hydroxybenzoic acid, 4–(diphenylamino)phenyl boronic acid, 2–aminothiophenol, $Pd(PPh_3)_4$, K_2CO_3, pyridine, acetic anhydride, KOH and NaH were purchased from Tokyo Chemical Industries (TCI), Japan. All the solvents used for the synthesis were from Wako Pure Chemical Industries Ltd., Japan. All the reagents were used without further purification.

Characterizations

All the synthesized compounds were purified by column chromatography on silica gel. Compounds **I**–**III** were purified by column chromatography followed by recycle preparative high performance liquid chromatography (HPLC) system (Japan Analytical Industry Co., Ltd., LC–9210NEXT with JaiGel–1H/–2H) using chloroform as eluent. The intermediates and compounds were characterized by ^{1}H–NMR, ^{13}C–NMR, MALDI–TOF (Matrix–assisted laser desorption ionization time–of–flight) and elemental analysis techniques. The ^{1}H–NMR spectra were recorded on a JEOL 400SS (400 MHz) spectrometer and all spectra were recorded in a $CDCl_3$ solvent using TMS as an internal reference standard at room temperature (20 °C). Chemical shifts of NMR spectra are given in parts per million (ppm). Low and high resolution matrix–assisted–laser–desorption/ionization (MALDI) mass spectra (MS) were obtained on Bruker Daltonics ultraflex using dithranol as a matrix. All steady state absorption spectra were recorded on a JASCO V–570 UV–Vis spectrophotometer. Fluorescence spectra were measured on fluorescence spectrophotometer (F–2700, Hitachi High–Technologies). Absolute quantum yields were measured on FP–6500 spectrofluorometer with an ISF–513 fluorescence integrate sphere unit (JASCO). The single crystals were obtained by slow evaporation of a mixed solution ($CHCl_3$: ethanol) for compounds **I** and **II** and data collections were performed on a Rigaku R–AXIS–RAPID diffractometer with Cu–Kα radiation (λ = 0.7107 Å) at –143 °C. DSC measurements were performed on a PerkinElmer model DSC 8000 differential scanning calorimeter. Powder-XRD measurements were performed on MiniFlex 600, Rigaku make in the range of 2θ = 2–30°. Atomic force microscopy (AFM) analyses were performed on Burker–co model–multimode–1–AFM. Opticoat spin coater MSA100 was used for spin–coating. All theoretical calculations were performed using Gaussian 09 package.

Synthesis Details

***2–(Benzo[d]thiazol–2–yl)–5–bromophenol* 3**

Phosphorus trichloride (0.63 g, 4.6 mmol) was added dropwise to a solution of 4–bromo–2–hydroxybenzoic acid (1.0 g, 4.6 mmol) and 2–aminothiophenol (0.69 g, 5.5 mmol) in toluene (40 mL), maintaining the temperature below 40 °C. The mixture was refluxed for 8 h, after completion of reaction; reaction mixture was neutralized with aqueous sodium carbonate solution (20% w/v). Toluene was removed by vacuum distillation and crude product was extracted from chloroform which was further purified by column chromatography on silica gel

(Hexane–ethylacetate: 90:10) to yield 2–(benzo[*d*]thiazol–2–yl)–5–bromophenol **3** as white solid[36]. Yield after column chromatography: 52%, white solid. ^{1}H–NMR (400 MHz, $CDCl_3$, 20 °C): δ ppm 12.70 (s, 1H), 7.97–7.99 (dd, 1H), 7.89–7.91 (dd, 1H), 7.49–7.54 (m, 2H), 7.40–7.44 (m, 1H), 7.29 (d, 1H), 7.10–7.07 (dd, 1H). MALDI–TOF (*m*/*z*): calculated: 304.95, found: 305.925.

***2–(Benzo[d]thiazol–2–yl)–5–bromophenyl acetate* 4**

Mixture of 2–(benzo[*d*]thiazol–2–yl)–5–bromophenol **3** (4.0 g, 13.1 mmol), pyridine (4.0 mL) and acetic anhydride (10 mL) were stirred in dichloromethane (80 mL) at room temperature for 24h. After completion of reaction, reaction mixture was quenched in ice and product was extracted with dichloromethane. The dichloromethane layer was concentrated under vacuum to yield crude 2–(benzo[*d*]thiazol–2–yl)–5–bromophenyl acetate **4** which was further purified by column chromatography on silica gel (Hexane–ethylacetate: 97:3). Yield after column chromatography: 58 %, white solid[36]. ^{1}H–NMR (400 MHz, $CDCl_3$, 20 °C): δ ppm 8.19–8.21 (d, 1H), 8.06–8.08 (dd, 1H), 7.91–7.93 (dd, 1H), 7.49–7.54 (m, 2H), 7.39–7.44 (m, 2H), 2.48 (s, 3H). MALDI–TOF (*m*/*z*): calculated: 348.21, found: 349.97

***4–(Benzo[d]thiazol–2–yl)–4'–(diphenylamino)–[1,1'–biphenyl]–3–yl acetate* I**

4–(Diphenylamino)phenyl boronic acid **5** (0.90 g, 3.1 mmol), 2–(benzo[*d*]thiazol–2–yl)–5–bromophenyl acetate **4** (1.2 g, 3.6 mmol), and $Pd(PPh_3)_4$ (0.015 g, 0.012 mmol) were added to a mixture of 60 mL degassed toluene (three times) and aqueous (degassed water 12 mL) 2 M K_2CO_3 under nitrogen atmosphere. The mixture was stirred at 115 °C for 22 h. After completion of reaction (monitored by thin layer chromatography) the mixture was cooled to room temperature, and poured into de-ionized water (200 mL). The aqueous layer was extracted thrice with dichloromethane. The combined organic layers were washed with water and dried over sodium sulfate. The organic layer was concentrated under vacuum, to obtain a green–yellow colored solid. The crude product was purified by column chromatography on silica gel (Hexane–ethylacetate: 90:10) followed by preparative recyclable HPLC (mobile phase: chloroform; 3mL/ min).

Yield after column chromatography: 64%, Green–yellow solid.

^{1}H–NMR (400 MHz, $CDCl_3$, 20 °C): δ ppm 8.34–8.36 (d, 1H), 8.07–8.10 (d, 1H), 7.92–7.94 (d, 1H), 7.58–7.60 (d, 1H), 7.51–7.53 (m, 3H), 7.38–7.44 (m, 2H), 7.25–7.29 (m, 4H), 7.12–7.15 (m, 6H), 7.06 (m, 2H), 2.51(s, 3H); ^{13}C–NMR (100 MHz, $CDCl_3$, 20 °C): δ ppm 169.30, 162.44, 153.07, 148.59, 148.16, 147.37, 143.98, 135.25, 132.36, 130.57, 129.36, 127.80, 126.32, 125.27, 124.75, 124.74, 124.33, 124.14, 123.31, 123.26, 121.40, 121.33, 21.86. MALDI–TOF (*m*/*z*): calculated: 512.16, found: 512.21; Elemental Analysis; Mol. Formula: $C_{33}H_{24}N_2O_2S$ (Actual: C: 77.32, H: 4.72, S: 6.26, N: 5.46; Found: C: 77.11, H: 4.69, S: 6.24, N: 5.49)

***4–(Benzo[d]thiazol–2–yl)–4'–(diphenylamino)–[1,1'–biphenyl]–3–ol* II**

4–(Benzo[*d*]thiazol–2–yl)–4'–(diphenylamino)–[1,1'–biphenyl]–3–yl acetate **I** (0.80 g, 1.5 mmol) was refluxed with potassium hydroxide (0.87g, 1.5 mmol) in dichloromethane (80 mL) for 12h. After completion of reaction (monitored by TLC) the mixture was cooled to room temperature, and poured into ice (200 g). The crude product was extracted thrice with dichloromethane. The combined organic layers were washed with water and dried over sodium sulfate. The organic layer was concentrated under vacuum, to obtain a yellow colored solid. The crude product **II** was purified by column chromatography on silica gel (Hexane–ethylacetate: 90:10) followed by preparative recyclable HPLC (mobile phase: chloroform; 3mL/ min).

Yield after column chromatography: 65%, yellow solid.

^{1}H–NMR (400 MHz, $CDCl_3$, 20 °C): δ ppm 12.56 (s, 1H), 7.98–8.00 (d, 1H), 7.90–7.91 (d, 1H), 7.71–7.73 (d, 1H), 7.49–7.55 (d, 3H), 7.39–7.42 (m, 2H), 7.26–7.32 (m, 4H), 7.12–7.20 (m, 7H), 7.04–7.07 (m, 2H); ^{13}C–NMR (100 MHz, $CDCl_3$, 20 °C): δ ppm 169.08, 158.17, 151.91, 148.03, 147.42, 144.97, 133.13, 132.53, 129.34, 128.80, 127.72, 126.67, 125.40, 124.73, 123.25, 122.05, 121.49, 117.90, 115.30, 115.17; MALDI–TOF (*m*/*z*): calculated: 470.58, found: 471.23; Elemental Analysis; Mol. Formula: $C_{31}H_{22}N_2OS$ (Actual: C: 79.12, H: 4.71, S: 6.81, N: 5.95; Found: C: 78.81, H: 4.58, S: 6.72, N: 5.83).

4'–(Benzo[d]thiazol–2–yl)–3'–methoxy–N,N–diphenyl–[1,1'–biphenyl]–4–amine III

4–(Benzo[d]thiazol–2–yl)–4'–(diphenylamino)–[1,1'–biphenyl]–3–ol **II** (0.05 g, 0.10 mmol) was stirred with methyl iodide (0.017 g, 0.12 mmol) in DMF in presence of NaH (0.003 g, 0.12 mmol) base for 1h. After completion of reaction (monitored by TLC) the reaction mass was quenched in ice. Yellow colored solid separated. The separated crude product was filtered, dried and purified by column chromatography on silica gel (Hexane-ethylacetate: 95:05).

Yield after column chromatography: 95%, green-yellow solid.

^{1}H–NMR (400 MHz, $CDCl_3$, 20 °C): δ ppm 8.56–8.58 (d, 1H), 8.08–8.10 (d, 1H), 7.92–7.94 (d, 1H), 7.53–7.55 (m, 2H), 7.47–7.51 (m, 1H), 7.33–7.39 (m, 2H), 7.24–7.31 (m, 6H), 7.14–7.16 (m, 5H), 7.04–7.08 (m, 2H), 4.12(s, 3H); ^{13}C–NMR (100 MHz, $CDCl_3$, 20 °C): δ ppm 162.99, 157.53, 152.24, 147.96, 147.46, 144.29, 136.07, 133.76, 129.83, 129.35, 127.82, 125.89, 124.65, 124.47, 123.47, 123.23, 122.66, 121,18, 120.75, 119.53, 109.65, 55.76; MALDI–TOF (*m*/*z*): calculated: 484.16, found: 484.22.

Acknowledgements

V. S. P. and D. S. thank the JSPS Research Fellowship. This work was partly supported by a Grant–in–Aid for Scientific Research (No. 2604063, 26102011, 26810023, 26102001) from the Japan Society for the Promotion of Science (JSPS).

Keywords: ESIPT • AIE • Molecular Packing • Fluorescence • Photophysics

[1] T. M. Figueira-Duarte, K. Müllen, *Chem. Rev.* **2011**, *111*, 7260.
[2] V. S. Padalkar, S. Seki, *Chem. Soc. Rev.* **2016**, *45*, 169.
[3] X.-H. Zhu, J. Peng, Y. Cao, J. Roncali, *Chem. Soc. Rev.* **2011**, *40*, 3509.
[4] K. Kumar, H. Duan, R. S. Hegde, S. C. W. Koh, J. N. Wei, J. K. W. Yang, *Nat. Nanotechnol.* **2012**, *7*, 557.
[5] B. Yoon, J. Lee, I. S. Park, S. Jeon, J. Lee, J.-M. Kim, *J. Mater. Chem. C* **2013**, *1*, 2388.
[6] R. Davis, N. S. SaleeshKumar, S. Abraham, C. H. Suresh, N. P. Rath, N. Tamaoki, S. Das, *J. Phys. Chem. C* **2008**, *112*, 2137.
[7] X. He, A. C. Benniston, H. Saarenpää, H. Lemmetyinen, N. V. Tkachenko, U. Baisch, *Chem. Sci.* **2015**, *6*, 3525.
[8] Y.-X. Li, J.-X. Qiu, J.-L. Miao, Z.-W. Zhang, X.-F. Yang, G.-X. Sun, *J. Phys. Chem. C* **2015**, *119*, 18602.
[9] T. Mutai, H. Satou, K. Araki, *Nat. Mater.* **2005**, *4*, 685.
[10] B. Kupcewicz, M. Małecka, *Cryst. Growth Des.* **2015**, *15*, 3893.
[11] M. Sen Yuan, D. E. Wang, P. Xue, W. Wang, J. C. Wang, Q. Tu, Z. Liu, Y. Liu, Y. Zhang, J. Wang, *Chem. Mater.* **2014**, *26*, 2467.
[12] Z. Zhang, B. Xu, J. Su, L. Shen, Y. Xie, H. Tian, *Angew. Chemie Int. Ed.* **2011**, *50*, 11654.
[13] Z. Zhao, Z. Wang, P. Lu, C. Y. K. Chan, D. Liu, J. W. Y. Lam, H. H. Y. Sung, I. D. Williams, Y. Ma, B. Z. Tang, *Angew. Chemie* **2009**, *121*, 7744.

[14] J. Ahn, S. Park, J. H. Lee, S. H. Jung, S.-J. Moon, J. H. Jung, *Chem. Commun. (Camb).* **2013**, *49*, 2109.
[15] S.-Y. Park, M. Ebihara, Y. Kubota, K. Funabiki, M. Matsui, *Dye. Pigment.* **2009**, *82*, 258.
[16] J. L. Scott, T. Yamada, K. Tanaka, *New J. Chem.* **2004**, *28*, 447.
[17] S. K. Rajagopal, A. M. Philip, K. Nagarajan, M. Hariharan, *Chem. Commun. (Camb).* **2014**, *50*, 8644.
[18] J. E. Kwon, S. Y. Park, *Adv. Mater.* **2011**, *23*, 3615.
[19] Y. Hong, J. W. Y. Lam, B. Z. Tang, *Chem. Soc. Rev.* **2011**, *40*, 5361.
[20] A. Mishra, M. K. R. Fischer, P. Bäuerle, *Angew. Chemie Int. Ed.* **2009**, *48*, 2474.
[21] Y. Ooyama, Y. Shimada, S. Inoue, T. Nagano, Y. Fujikawa, K. Komaguchi, I. Imae, Y. Harima, *New J. Chem.* **2011**, *35*, 111.
[22] A. Hagfeldt, G. Boschloo, L. Sun, L. Kloo, H. Pettersson, *Chem. Rev.* **2010**, *110*, 6595.
[23] P. Xue, P. Chen, J. Jia, Q. Xu, J. Sun, B. Yao, Z. Zhang, R. Lu, *Chem. Commun. (Camb).* **2014**, *50*, 2569.
[24] Y. Gong, Y. Tan, J. Liu, P. Lu, C. Feng, W. Z. Yuan, Y. Lu, J. Z. Sun, G. He, Y. Zhang, *Chem. Commun. (Camb).* **2013**, *49*, 4009.
[25] Y. H. Kim, S.-G. Roh, S.-D. Jung, M.-A. Chung, H. K. Kim, D. W. Cho, *Photochem. Photobiol. Sci.* **2010**, *9*, 722.
[26] V. S. Padalkar, D. Sakamaki, N. Tohnai, T. Akutagawa, K. Sakai, S. Seki, *RSC Adv.* **2015**, *5*, 80283.
[27] J. Cheng, D. Liu, W. Li, L. Bao, K. Han, *J. Phys. Chem. C* **2015**, *119*, 4242.
[28] C. Hsieh, P. Chou, C. Shih, W. Chuang, M. Chung, J. Lee, T. Joo, **2011**, 2932.
[29] M. Cai, Z. Gao, X. Zhou, X. Wang, S. Chen, **2012**, 5289.
[30] W.-T. Chuang, C.-C. Hsieh, C.-H. Lai, C.-H. Lai, C.-W. Shih, K.-Y. Chen, W.-Y. Hung, Y.-H. Hsu, P.-T. Chou, *J. Org. Chem.* **2011**, *76*, 8189.
[31] M. Ikegami, T. Arai, *J. Chem. Soc. Perkin Trans. 2* **2002**, 1296.
[32] M. Shimizu, Y. Takeda, M. Higashi, T. Hiyama, *Angew. Chemie - Int. Ed.* **2009**, *48*, 3653.
[33] H.-Y. Wang, G. Chen, X.-P. Xu, S.-J. Ji, *Synth. Met.* **2010**, *160*, 1065.
[34] Z.-Q. Liang, X.-M. Wang, G.-L. Dai, C.-Q. Ye, Y.-Y. Zhou, X.-T. Tao, *New J. Chem.* **2015**, *39*, 8874.
[35] D. Gudeika, J. V Grazulevicius, D. Volyniuk, G. Juska, V. Jankauskas, G. Sini, **2015**.
[36] V. S. Padalkar, D. Sakamaki, K. Kuwada, N. Tohnai, T. Akutagawa, K. Sakai, S. Seki, *RSC Adv.* **2016**, *6*, 26941.
[37] G. Singh, V. Bhalla, M. Kumar, *Phys. Chem. Chem. Phys.* **2015**, *17*, 22079.
[38] B. J. Cornil, D. Beljonne, J. Calbert, J. Brødas, J. Cornil, D. Beljonne, J. Calbert, J.-L. Brédas, *Adv. Mater.* **2001**, *13*, 1053.
[39] J. Chen, C. C. W. Law, J. W. Y. Lam, Y. Dong, S. M. F. Lo, I. D. Williams, D. Zhu, B. Z. Tang, *Chem. Mater.* **2003**, *15*, 1535.
[40] T. Jadhav, B. Dhokale, S. M. Mobin, R. Misra, *RSC Adv.* **2015**, *5*, 29878.
[41] Y. Zhang, J. Sun, G. Bian, Y. Chen, M. Ouyang, B. Hu, C. Zhang, *Photochem. Photobiol. Sci.* **2012**, *11*, 1414.
[42] M. Yang, D. Xu, W. Xi, L. Wang, J. Zheng, J. Huang, J. Zhang, H. Zhou, J. Wu, Y. Tian, *J.Org. Chem*. **2013,** 78, 10344.
[43] M. Frish, H. B. Trucks, H. B. Schlegel, G. S. Scuseria, M. A. Robb, J. R. Cheeseman, G. Scalmani, V. Barone, B. Mennucci and G. A. Paterson, Guassian 09, revision 02, Inc. Wallingford CT, 2009, p34.

FULL PAPER

Influence of molecular packing on solid state emission properties of ESIPT and non-ESIPT motifs is discussed in detail.

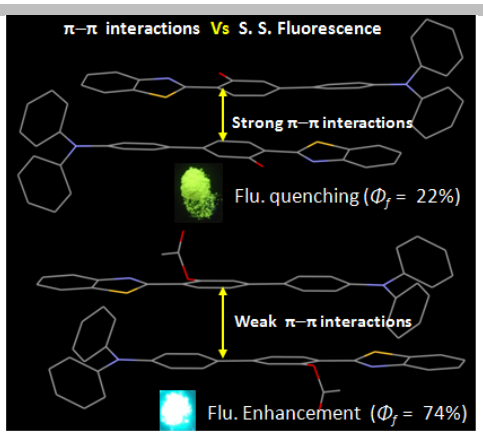

V. Padalkar, D.Sakamaki, K. Kuwada, A. Horio, H. Okamoto, N. Tohnai, T. Akutagawa, A. Sakai, S. Seki**

Page 1. – Page 7.

Title: π–π Interactions: Influence on molecular packing and solid state emission of ESIPT and non–ESIPT motifs